Nanoscale Advances

ROYAL SOCIETY OF CHEMISTRY

PAPER

View Article Online
View Journal | View Issue

Cite this: *Nanoscale Adv.*, 2024, **6**, 3064

An integrated design strategy coupling additive manufacturing and matrix-assisted pulsed laser evaporation (MAPLE) towards the development of a new concept 3D scaffold with improved properties for tissue regeneration

Teresa Russo,†[a] Valentina Peluso,†[a] Antonio Gloria,*[b] Valentina Gargiulo,[c] Michela Alfe *[c] and Giovanni Ausanio*[d]

Bioinspired strategies for scaffold design and optimization were improved by the introduction of Additive Manufacturing (AM), thus allowing for replicating and reproducing complex shapes and structures in a reliable manner, adopting different kinds of polymeric and nanocomposite materials properly combined according to the features of the natural host tissues. Benefiting from recent findings in AM, a Matrix-Assisted Pulsed Laser Evaporation (MAPLE) technique was employed for obtaining graphene-like material (GL) uniform coatings on 3D scaffolds for tissue repair strategies, towards the development of a new concept 3D scaffold with controlled morphological/architectural and surface features and mechanical and biological properties. The effect of the material-design combination through an integrated technological approach (*i.e.*, MAPLE deposition of GL on 3D AM PCL scaffolds) was assessed through scanning electron microscopy, atomic force microscopy, contact angle measurements, mechanical measurements and biological analyses (cell viability assay and alkaline phosphatase activity) in conjunction with confocal laser scanning microscopy. The differentiation of hMSCs towards the osteoblast phenotype was also investigated analysing the gene expression profile. The obtained findings provided a further insight into the development of improved strategies for the functionalization or combination of GL with other materials and 3D structures in a hybrid fashion for ensuring a tighter adhesion onto the substrates, improving cell fate over time, without negatively altering the mechanical properties and behaviour of the neat constructs. In particular, the results provided interesting information, making 3D AM GL-coated scaffolds potential candidates for bone tissue engineering.

Received 31st January 2024
Accepted 12th April 2024

DOI: 10.1039/d4na00098f

rsc.li/nanoscale-advances

1. Introduction

The introduction of additive manufacturing (AM) technologies has led to a strong improvement in developing 3D constructs replicating the functional architecture and complex structure of native tissues and organs.[1,2]

AM technologies operate in a layer-by-layer fashion and are crucial for the design of 3D scaffolds with controlled morphological and architectural features as well as fully interconnected pore networks.[3–5]

AM techniques based on injection/extrusion methods (*e.g.*, 3D fiber deposition) may involve the possibility of processing both acellular and cellular materials into biological constructs for disease modelling, tissue engineering or regenerative medicine applications.[3–7]

Even though the great potential of 3D bioprinting techniques can be considered as not fully explored, many systems are currently favouring a gradual shift with regard to the clinical landscape. In this context, the combination of image capture and analysis techniques with AM should enhance the fabrication of patient-specific devices showing a better performance in terms of tissue regeneration.[5,7]

Among synthetic polymers employed in biomedicine, aliphatic polyesters and in particular poly(ε-caprolactone) (PCL) are widely investigated. PCL is a semi-crystalline and Food and Drug Administration (FDA)-approved polymer generally

[a]*Institute of Polymers, Composites and Biomaterials, National Research Council of Italy, 80125 Naples, Italy*

[b]*Department of Industrial Engineering, University of Naples Federico II, 80125 Naples, Italy. E-mail: antonio.gloria@unina.it*

[c]*Institute of Sciences and Technologies for Sustainable Energy and Mobility (STEMS), National Research Council of Italy, 80125 Naples, Italy. E-mail: michela.alfe@stems.cnr.it*

[d]*Dipartimento di Fisica "Ettore Pancini", Università degli Studi di Napoli Federico II, 80125 Napoli, Italy. E-mail: giovanni.ausanio@unina.it*

† Both first authors.

employed to manufacture scaffolds for tissue regeneration, as a consequence of its biocompatibility, long lasting mechanical characteristics and degradation features.[8]

Over the past few years, the use of hydroxyapatite (HA), magnetite (Fe_3O_4) or iron-doped hydroxyapatite (FeHA) nanoparticles[8–13] has also been considered for the development of 3D AM nanocomposite (PCL/HA, PCL/Fe_3O_4, and PCL/FeHA) scaffolds with integrated functionalities for enhanced bone tissue engineering, providing interesting results.[14–17]

Great efforts have been made to push the research towards the identification of novel materials, innovative methodological approaches and technologies aiming to design 3D devices with peculiar properties.

From a materials science point of view, carbon-based and in particular graphene-related materials (GRMs) are emerging biocompatible coatings.[18] GRMs comprise a wide pool of materials differing in terms of the structure (few-layer and multi-layered structures), composition and properties (even within the same GRM category). In addition to graphite, C-based sources for GRM production include carbon black, coke, carbonized/pyrolyzed wastes, biomasses and organic bio-precursors (*e.g.* plant-based, amino acids, and carbohydrates) through many approaches (*e.g.* thermal decomposition, ball milling, microwave sintering, flash Joule heating (FJH), hydrothermal methods, template-based confinement method and combined approaches).[19–27]

Graphene-like materials (GL) obtained from a top-down demolition of a nanostructured carbon black exhibit antimicrobial activity toward living cells through a bacteriostatic action[28] and a proven biocompatibility on a vertebrate model.[29] GL was further inspected[30] by a biological survey toward target cellular lines (murine fibroblast NIH3T3, human keratinocytes HaCAT and the human cervical adenocarcinoma epithelial-like HeLa) demonstrating no perturbations in the different biological parameters evaluated, including the cytotoxic potential. GL composites are also capable of allowing Murine Embryonic Stem Cell (ESC) and Rat Microglial Cell (MC) growth and prolification.[31] Furthermore, a very recent study successfully tested the compatibility of GL hybrids with neuron and beating cardiomyocyte differentiation.[32]

For the above reported evidence, GRMs (and specifically GL) can be considered as interesting coatings for several devices in biomedical applications,[33,34] even if the studies on such coatings are still in their early stages.

The control of coating uniformity and thickness results in a crucial feature concerning the surface coating. Currently, there are many approaches for finely tailoring the surface chemistry and characteristics of coatings (*e.g.*, physical vapor deposition, chemical and photochemical deposition, dip-coating, spin coating, and sputtering deposition).[35]

However, such techniques generally lead to inappropriate adherence related to the use of solvents.

A strict control of the coating and a good adherent film may be achieved benefiting from technological advances. In this scenario, the matrix-assisted pulsed laser evaporation (MAPLE) technique would be one of the intriguing and efficient options, as it represents a solvent-free technique especially employed to obtain ultra-thin, homogeneous and well adherent coatings on different kinds of substrates, without altering the physical and chemical properties of the deposited material.[30,36,37]

MAPLE can also allow coating nonplanar substrates with specific biomolecules and drugs, while maintaining their activity and peculiar features.[30,36,37] Consequently, MAPLE ensures an optimal design of surface properties in terms of coating adhesion on the biomedical surface, and a better control over antibacterial properties can be achieved in many cases.[30]

For the first time MAPLE was recently employed to deposit GL on silicone slices, and the potential use as a functional coating was investigated for invasive devices for specific medical applications (*i.e.*, indwelling urinary catheters). Specifically, interesting results were already obtained through coating of flexible polydimethylsiloxane (PDMS) substrates using MAPLE with GL,[30] thus providing a further insight into the development of improved strategies for the functionalization or combination of GL with other materials in a hybrid fashion for ensuring a tighter adhesion onto the substrates.

Accordingly, benefiting from the previous results, the aim of the current research was to develop a new concept 3D scaffold (*i.e.*, GL-coated PCL) with controlled morphological/architectural and surface features and mechanical and biological properties, through the material-design combination using an integrated technological approach (AM and MAPLE).

Contact angle measurements, and morphological/topographical, mechanical and preliminary biological analyses were performed to assess the effect of GL coating on the performance of 3D AM scaffolds as well as the feasibility of the integrated technological approach.

2. Materials and methods

2.1. 3D scaffold design and preparation

2.1.1. Preparation of 3D AM scaffolds and GL suspension for MAPLE deposition. Poly(ε-caprolactone) (PCL, Mw = 65 000, Sigma-Aldrich, St. Louis, MO) pellets were used and 3D scaffolds (length l_0 of 10.0 mm, width w_0 of 10.0 mm, and height h_0 of 7.0 mm) were fabricated by the Fused Deposition Modeling/3D fiber deposition technique, using an extrusion-based system (EnvisionTEC GmbH, Germany). The pellets were heated to 100 °C and the 3D scaffolds were built layer by layer. A nitrogen pressure of 8.0 bar was employed for the processing of the material. The molten polymer was extruded/injected through a needle with an inner diameter of 400 μm. The filaments were deposited according to a lay-down pattern of 0/90°. A fiber spacing (*i.e.*, centre-to-centre distance between two fibers) and a layer thickness of 750 and 320 μm were employed, respectively. A deposition speed of 40 mm min^{-1} was used.

GL nanoparticles were prepared by means of a top-down demolition of a nanostructured carbon black (furnace type, CB N110, provided by Sid Richardson Carbon Co., Fort Worth, TX, USA) according to a previously reported approach.[30,38] Briefly, carbon black powder (500 mg) was ground in a mortar and treated under stirring and reflux for 90 h with 10 mL of

concentrated nitric acid (HNO_3, 67%) at 100 °C. After the oxidation step the recovered sample was reduced with hydrazine hydrate (35 μL of hydrazine hydrate for each mg of sample) at 100 °C under stirring and reflux for 24 h. Following the reduction step, the hydrazine excess was neutralized with diluted nitric acid and the reduced sample (hereinafter GL) was recovered by centrifugation and further purified from reactant traces by under-vacuum filtration (Durapore® Membrane Filter, 0.22 μm). The GL, recovered on the filter, was diluted with distilled water establishing a concentration of 1 wt% (0.01 g mL^{-1}) and stored. Before use, the GL suspension was treated by ultrasonic agitation (15 min at room temperature) to ensure concentration homogeneity before each deposition.

2.1.2. Preparation of 3D AM GL-coated scaffolds using MAPLE deposition. The MAPLE set-up was detailed elsewhere.[30] The adopted configuration comprises a Nd:YAG operated at its fundamental wavelength (1064 nm), a vacuum chamber and two pumps (a rotary pump for bootstrap and a turbomolecular pump for high vacuum). The target holder consists of a copper vessel (around 2 mL capacity). The GL suspension was poured in the target holder, quickly frozen through immersion in liquid nitrogen, and placed into a vacuum chamber and in thermal contact with a liquid nitrogen reservoir. The temperature at the MAPLE target, measured with a thermocouple, was about −133 °C. The substrate (3D AM scaffold) was placed at a distance of 8 mm from the target and the vacuum chamber was evacuated establishing a constant pressure inside the chamber ($\sim 10^{-6}$ torr). The laser beam reached the target at 45° and was partially focused to an ellipsoidal area of about 1.0 mm × 1.4 mm. The target was continuously moved with a 2D translation allowing the laser beam to scan a target area of about 1.5 cm^2. The deposition of GL on the 3D AM scaffold was obtained by adopting the following laser parameters: pulse repetition rate 4 Hz, pulse duration 7 ns, and laser pulse energy 350 mJ per pulse (corresponding to a fluence of $F = 25$ J cm^{-2}). Given the characteristic absorption in the visible region of the GL,[38,39] it is worth noting that the adopted values of laser fluence are well consistent with inverse matrix-assisted pulsed laser evaporation (IMAPLE) deposition conditions,[40] where the GL acts as a "self-matrix" thus allowing an efficient desorption of the frozen suspension in water without the use of light-absorbing solvents acting as a matrix (typically toluene) in the classic MAPLE desorption process.

2.2. Surface morphology and topography analysis

Scanning Electron Microscopy (SEM) was employed to analyse GL as well as PCL scaffolds after MAPLE deposition treatment, using a FEI Quanta 200 FEG apparatus (The Netherlands). Before analysis, all samples were capped with a thin conductive gold layer.

Atomic Force Microscopy (AFM) was performed on flat PCL substrates using an AFM Digital Instruments Nanoscope IIIa equipped with a sharpened silicon tip with a radius of less than 10 nm. The images of the surface profiles were obtained by operating the microscope in the tapping mode, with a scan size and rate of 2 μm and 1 Hz, respectively.

2.3. Contact angle measurements

Contact angle measurements were conducted on PCL and GL-coated PCL membranes by means of DATAPHYSICS OCA 20 apparatus, using deionized water and methylene iodide. The liquids were added dropwise on the membranes in different sites and the contact angle was assessed. CCD cameras recorded the process of the droplet addition on the membrane. The drop profile was extracted as already reported in the literature.[41–43] Contact angles and surface free energy were evaluated and reported as mean value ± standard deviation.

2.4. Mechanical measurements

Mechanical compression tests were performed on two different kinds of 3D AM scaffolds (PCL and GL-coated PCL), using an INSTRON 5566 testing machine. Specifically, the block-shaped specimens ($l_0 = 10.0$ mm, $w_0 = 10.0$ mm and $h_0 = 7.0$ mm) were compressed to a strain of 20% at a rate of 1 mm min^{-1}.

The engineering stress (σ) and strain (ε) were calculated as reported below:

$$\sigma = \frac{F}{A_0}$$

$$\varepsilon = \frac{\Delta h}{h_0}$$

where F is the measured force, A_0 ($l_0 \times w_0$) represents the initial cross-section area of the specimen, and Δh and h_0 are the height variation and the initial height of the specimen, respectively.

2.5. Cell culture

Bone marrow human mesenchymal stem cells (hMSCs, Millipore, Germany) were cultured in Dulbecco's modified eagle medium (DMEM, Microtech, Italy) supplemented with 10% (v/v) fetal bovine serum (FBS, Gibco, Thermo Fisher Scientific, Waltham, MA, USA), 2 mM glutamine, and antibiotics (penicillin G sodium 100 U mL^{-1} and streptomycin 100 g mL^{-1}) at 37 °C and 5% CO_2.

PCL and GL-coated PCL scaffolds were prepared by soaking the structures in a solution of ethanol and antibiotics (penicillin/streptomycin), washed in phosphate-buffered saline (PBS, Sigma-Aldrich, Milan, Italy), and pre-wetted in FBS. hMSCs were seeded onto the scaffolds using a density of 1.0×10^5 cells per sample. After seeding, the cell-laden structures were incubated for 2 h (37 °C and 5% CO_2) and, successively, 1.5 mL of culture medium was added to each well in a 48-well plate.

2.6. Cell viability assay

Alamar Blue assay (AbD Serotec Ltd., UK) was used to assess cell viability and proliferation. At 3, 7, 14, and 21 days after cell seeding, the cell-laden scaffolds were rinsed with PBS (Sigma-Aldrich, Italy) and 200 μL of DMEM without phenol red (HyClone, UK) containing 10% (v/v) Alamar Blue was added for each sample. The samples were incubated in a 5% CO_2 diluted atmosphere for 4 h at 37 °C.

After removing one hundred microliters of the solution, it was transferred to a well plate. A spectrophotometer (Sunrise, Tecan, Männedorf, Zurich, Switzerland) was utilized, and the optical density was measured at wavelengths of 570 and 595 nm. The experiments were done at least three times in triplicate.

2.7. Alkaline phosphatase activity

Samples were removed from the medium and washed twice with PBS on days 7, 14 and 21. The PCL and GL-coated PCL cell-laden scaffolds were then incubated in 1 mL of a lysis buffer and centrifugated. A cell density of 1.0×10^5 cells per sample was employed.

The alkaline phosphatase (ALP) activity was measured with an enzymatic assay (SensoLyte pNPP alkaline phosphatase assay kit – AnaSpec Inc., Fremont, CA, USA), which was based on *p*-nitrophenyl phosphate (*p*NPP). According to the manufacturer's protocol, the working solutions were prepared, and the procedure was followed.

2.8. Confocal laser scanning microscopy

Confocal laser scanning microscopy (CLSM) was also employed as an optical imaging technique for the analysis of cell adhesion and spreading at 14 and 21 days after seeding, using a Zeiss LSM 510/ConfoCor 2 system (Oberkochen, Germany) equipped with argon and helium–neon lasers and with a 10× and 20× objective. Cells were fixed with 4% paraformaldehyde for 20 min at room temperature, and permeabilized in 0.5% Triton-X100 and 1% BSA in PBS for 10 minutes. Actin filaments were stained with Phalloidin-AttoRho6G (100 μm), all from Sigma-Aldrich. Phalloidin fluorescence was collected in a spectral window of 500 to 530 nm.

2.9. Gene expression profile

The extraction of total RNA was carried out using a Total RNA Purification Plus Kit. The isolation of the total RNA samples and qRT-PCR assays were performed using a Bio-Rad CFX96 Real-Time PCR System (Hercules, CA, USA), according to the procedures already reported in the literature.[44]

The expression of osteogenesis-related genes including runt-related transcription factor 2 (RUNX2), osteopontin (OPN) and osteocalcin (OC) was analysed on days 7, 14 and 21. Data analysis was conducted using a method described in the literature.[44]

The obtained results were reported as fold change of target genes on GL-coated PCL compared with neat PCL (as control).

2.10. Statistical analysis

Each experiment was repeated at least three times in triplicate unless otherwise stated. The results were reported as mean value ± standard deviation. Statistical analysis was performed by one-way or two-way ANOVA, followed by the Bonferroni test with multiple comparisons among the distinct groups. The results were evaluated as statistically significant considering different confidence levels.

3. Results

3.1. Scanning electron microscopy

SEM images of the GL-coated PCL scaffolds are reported in Fig. 1. The surface morphological and topographical features of the nanocomposites were clearly influenced by the presence of GL deposits that appeared well distributed on the scaffold fibre as well as inside the pores of the morphologically controlled scaffold.

This evidence confirms the suitability of the MAPLE technique for the production of well-adherent coatings on complex 3D scaffolds. Its higher versatility allows for the deposition of delicate compounds (*e.g.*, proteins or polymers) in the form of thin films without altering the stability of their functional characteristics.[45] This important aspect is particularly evident when MAPLE is used on cryogenic targets made from the compounds of interest in an appropriate solvent.

The laser beam hits the target placed in the vacuumed deposition chamber and transfers the compounds without any damage.

The surface morphology and topography of the GL-coated PCL scaffolds were also inspected by AFM and compared with neat PCL. The AFM images (Fig. 2) demonstrated that the surface of the PCL substrate was completely covered by GL without discontinuity at the nanometric level.

The surface roughness parameters of GL-coated PCL scaffolds have been estimated (mean roughness, Ra, and Root Mean Square, RMS) and compared with those of bare PCL. The results were Ra = 41 ± 3 nm and RMS = 50 ± 4 nm for the GL-coated PCL scaffolds and Ra = 21 ± 3 nm and RMS = 30 ± 2 nm for the PCL. The higher RMS detected for the GL-coated PCL scaffolds is consistent with the MAPLE deposition characteristics where clusters of dry GL impacted the substrate without any settlement due to typical GL self-assembling phenomena arising upon slow drying from water suspension.[46]

3.2. Contact angle measurements

Contact angle testing provided information on the wettability and surface free energy. In particular, Table 1 reports the water

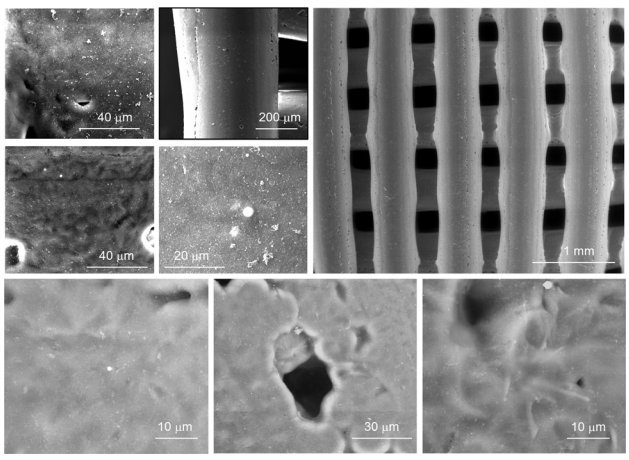

Fig. 1 SEM images of GL-coated PCL scaffolds at different magnification.

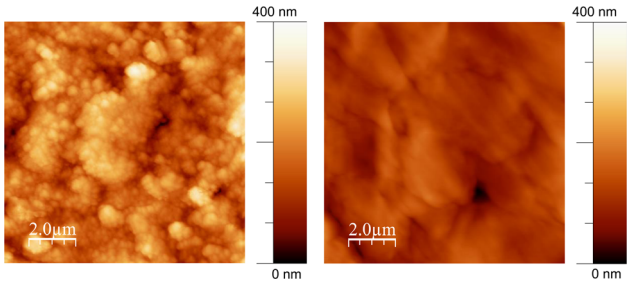

Fig. 2 Non-contact representative AFM images (10 μm × 10 μm) of GL-coated PCL scaffolds (left) and the PCL substrate (right).

Table 1 Results from contact angle measurements: water contact angle and surface free energy reported as mean value ± standard deviation

Membrane	Water contact angle (°)	Surface free energy (mJ m^{-2})
PCL	89.1 ± 1.0	42.3 ± 1.1
GL-coated PCL	75.5 ± 0.7	48.1 ± 1.0

contact angle and surface free energy in the case of PCL and GL-coated PCL membranes.

The water contact angles obtained for GL-coated PCL (75.5 ± 0.7°) were significantly lower than those obtained for neat PCL (89.1 ± 1.4°). As a consequence, GL-coated PCL structures appear to be significantly more hydrophilic than the PCL counterparts.

The presence of the GL coating led to a significant increase in the surface free energy.

3.3. Mechanical measurements

The mechanical compression tests performed on the two kinds of scaffolds showed a behaviour similar to that already reported in the literature for 3D AM scaffolds.[5,14] Fig. 3 reports the typical stress–strain curves obtained for PCL and GL-coated PCL scaffolds.

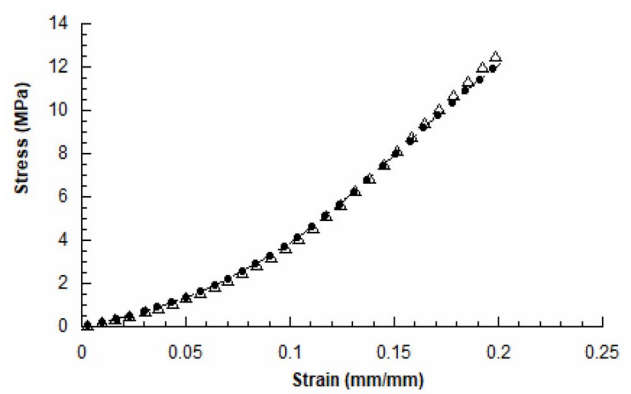

Fig. 3 Typical stress–strain curves obtained for 3D AM PCL (●) and GL-coated PCL (△) scaffolds (rate of 1 mm min^{-1} and final strain of 20%).

Table 2 Mechanical properties of 3D AM PCL and GL-coated PCL scaffolds: compressive modulus (E) and maximum stress (σ_{max})

3D AM scaffold	E (MPa)	σ_{max} (MPa)
PCL	27.5 ± 2.1	12.3 ± 0.6
GL-coated PCL	27.8 ± 2.0	12.9 ± 0.7

The compressive modulus was evaluated as the slope of the initial linear region of the stress–strain curve. The compressive modulus (E) and maximum stress (σ_{max}) were reported as mean value ± standard deviation (Table 2).

In particular, the neat PCL scaffolds showed a compressive modulus of 27.5 ± 2.1 MPa and a maximum stress of 12.3 ± 0.6 MPa, whilst values of 27.8 ± 2.0 MPa and 12.9 ± 0.7 MPa were obtained for the GL-coated PCL structures. However, no statistically significant differences ($p > 0.05$) were found between the two groups, in terms of compressive modulus and maximum stress. Thus, the presence of the functional GL coating did not significantly affect the mechanical properties and behaviour of the 3D PCL constructs.

3.4. Cell viability assay

All samples supported the adhesion and proliferation of hMSCs. As reported, the number of viable cells was associated with the magnitude of dye reduction. A significant increase of Alamar Blue reduction was evident for PCL and GL-coated PCL scaffolds up to 14 days after seeding (Fig. 4). The results indicated that hMSCs were viable on both PCL and GL-coated PCL scaffolds. However, even though on day 3 no statistically significant differences were observed between the two groups, higher values of Alamar Blue reduction were found for GL-coated PCL scaffolds on 7, 14 and 21 days, compared to the neat PCL structures.

3.5. Alkaline phosphatase activity (ALP)

The alkaline phosphatase activity was measured on 7, 14 and 21 days for each group (PCL and GL-coated PCL). Fig. 5 reports

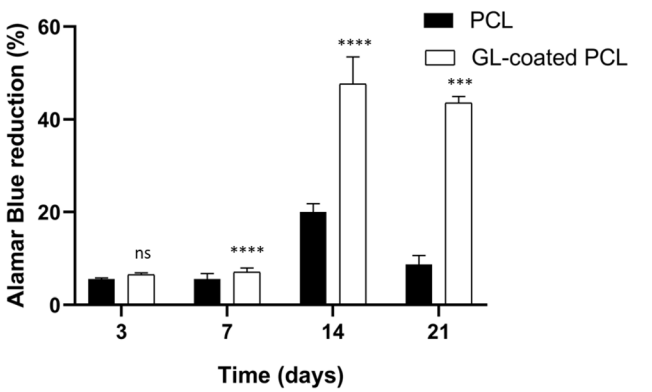

Fig. 4 Percentage of Alamar Blue reduction evaluated for PCL and GL-coated PCL scaffolds at different time points. Statistical analysis was performed by two-way ANOVA followed by the Bonferroni test with multiple comparisons. (ns, ***$p < 0.001$, and ****$p < 0.0001$).

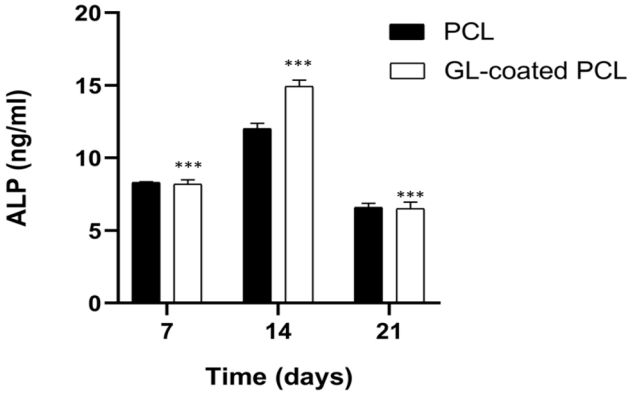

Fig. 5 Alkaline phosphatase (ALP) activity for PCL and GL-coated PCL scaffolds at 7, 14 and 21 days after cell seeding. Statistical analysis was performed by two-way ANOVA followed by the Bonferroni test with multiple comparisons. (ns, ***$p < 0.001$, and ****$p < 0.0001$). The values were all statistically significant compared to PCL at each time point.

some differences in terms of results. ALP peaked at 14 days after seeding. However, at each time point, the GL-coated PCL scaffolds showed significantly higher values of ALP activity, in comparison to the PCL ones. Accordingly, the presence of the GL coating strongly improved ALP activity.

3.6. Confocal laser scanning microscopy

CLSM performed on cell-laden structures at 14 and 21 days after seeding provided qualitatively results in terms of cell adhesion and spreading over the observation time. The number of viable cells seems to increase over time (Fig. 4) with some modifications in the morphology, changing from a geometry characterized by a few ramifications to a thread-like geometry, with an increased number of ramifications. Cells appeared uniformly distributed on both PCL and GL-coated PCL scaffold surfaces. However, a better spreading was evident in the case of GL-coated PCL scaffolds (Fig. 6).

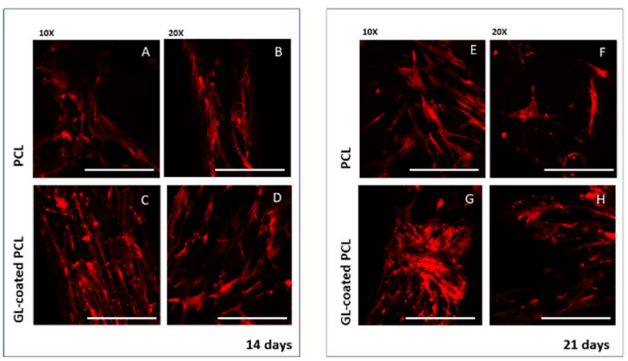

Fig. 6 Confocal laser scanning microscopy (CLSM) analysis on cell-laden scaffolds at different time points. Images of rhodamine phalloidin-stained actin filaments. A–D 14 days (A–C-10× magnification, scale bar 250 μm; B–D 20× magnification, scale bar 500 μm); E–H 21 days (E–G 10× magnification, scale bar 250 μm; F–H 20× magnification, scale bar 500 μm).

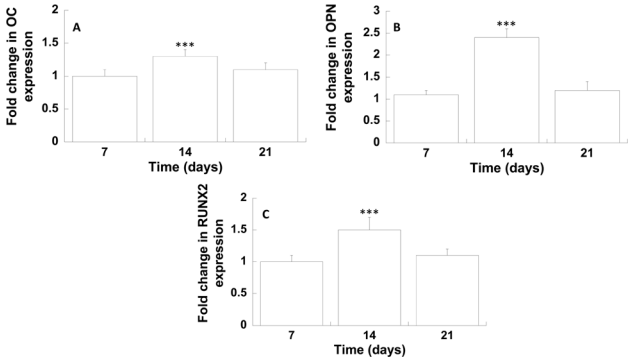

Fig. 7 Results from gene expression profile of osteogenic markers – (A) osteocalcin (OC); (B) osteopontin (OPN); (C) runt-related transcription factor 2 (RUNX2). Statistical analysis was performed by two-way ANOVA followed by the Bonferroni test with multiple comparisons. (ns, ***$p < 0.001$, and ****$p < 0.0001$).

3.7. Gene expression profile

The differentiation of hMSCs towards the osteoblast phenotype on GL-coated PCL surfaces was investigated analysing the gene expression profile (Fig. 7).

On day 14, the results showed a significantly improved mRNA expression level of OC and OPN, compared to the neat PCL. Analogously, on day 14, with regard to the transcription factor RUNX2, in the case of GL-coated PCL structures, the level was 1.5 (±0.2) fold higher than that of the neat PCL.

4. Conclusions

Graphene-like materials (GL) were obtained from a top-down demolition of a nanostructured carbon black and adopted as antimicrobial and biocompatible coatings of 3D morphologically controlled scaffolds fabricated in a layer-by-layer fashion by means of an Additive Manufacturing (AM) technique, with the aim to propose an integrated strategy for finely tuning scaffold features for tissue repair and regeneration.

As frequently reported, the control of coating uniformity and thickness clearly remains a fundamental aspect for surface coating. The matrix-assisted pulsed laser evaporation (MAPLE) technique was adopted as an intriguing and efficient solvent-free option to obtain ultra-thin, homogeneous and well adherent coatings, without altering the physical and chemical properties of the deposited material, allowing coating complex and nonplanar objects with specific biomolecules and drugs also maintaining their activity and peculiar features.[30,36,37]

Accordingly, benefiting from the previous results, the current research was properly pursued to develop a new concept 3D scaffold with controlled properties through the material-design combination using an integrated technological approach (*i.e.*, MAPLE deposition of GL on 3D AM PCL scaffolds). The results obtained from SEM analysis revealed a uniform GL coating onto the fiber of the 3D scaffolds, also highlighting that the GL coating was visible on the fibers of the deeper layers of 3D AM scaffolds. On the other hand, compression tests performed on PCL and GL-coated PCL scaffolds confirmed that the presence of the GL coating did not

negatively alter the mechanical properties and behaviour of the 3D PCL scaffolds. Furthermore, the results from biological measurements highlighted that hMSCs were viable on both PCL and GL-coated PCL scaffolds. However, higher values of Alamar Blue reduction (on 7, 14 and 21 days) and alkaline phosphatase activity were found for GL-coated PCL scaffolds. In particular, at each time point, the higher ALP values found for the GL-coated scaffolds suggested that the material-design combination through the integrated technological approach provided the possibility of developing a new concept 3D scaffold able to better support the osteogenic differentiation of hMSCs.

Such results were also in good agreement with those from CLSM analysis which showed cell morphological changes.

On the other hand, even though water contact angle data provide important information on the surface wettability, the surface free energy clearly affects further surface features and properties. The surface free energy represents an important parameter which characterises the solid surface as well as the interaction with other materials.[47] This parameter is related to the wettability and to further fundamental properties at the surface interface (*e.g.*, adhesion and friction). Thus, its values are important for the application of the analysed materials according to different fields.[47]

In the biomedical field, scientific studies on the effects of cell attachment and differentiation were already carried out by measuring the wettability and surface free energy, also reporting that hydrophilic substrates with high surface free energy resulted in high biocompatibility and osteogenic responses.[48]

Accordingly, in the current work, the contact angle measurements were in agreement with those obtained from cell viability assay, ALP activity and CLSM analysis. Specifically, it was demonstrated that the structure with higher hydrophilicity and free energy (*i.e.*, GL-coated PCL) improved cell adhesion, spreading and differentiation, differently from a surface with low free energy, which could also inhibit cell behavior in many cases. Thus, the improved wettability led to a better cell spreading, even if the role of the surface free energy should also be considered as the adhesion depends on the polar and nonpolar components of the surface free energy; in particular, the polar component mainly affects the polar molecules (*e.g.*, water and proteins).[49]

For this reason, the wettability and surface free energy could represent an important indicator of cell behavior to guide the design and development of AM scaffolds. However, it is worth noting that the combination of such properties with the surface topography clearly represents a further important feature. Indeed, the role of surface topography combined with those of the wettability and surface free energy has been frequently stressed in the literature.[49] For this reason, AFM was also performed, highlighting differences in terms of roughness (Ra = 41 ± 3 nm and RMS = 50 ± 4 nm for the GL-coated PCL scaffolds and Ra = 21 ± 3 nm and RMS = 30 ± 2 nm for the PCL).

Even though the stability/resistance of the GL deposits was also preliminarily assessed as the GL-coated samples (in the form of 3D porous scaffolds and 2D membranes) were immersed in the cell medium (see 2.5. Cell culture) and then digitally imaged at each time point (7, 14 and 21 days) and compared with those before the immersion (data not shown), nano-scratch tests should be performed to analyse the adhesion of the coating to the substrate.

The gene expression profile of osteogenic markers was employed to analyse the differentiation of hMSCs towards the osteoblast phenotype on GL-coated PCL surfaces. On day 14, the gene expression of OC and OPN, which are the major non-collagenous proteins secreted by pre-osteoblasts and osteoblasts,[50] was significantly enhanced. It is well known how these proteins play an important role in the deposition and organization of the bone matrix. Furthermore, on day 14, a significant increase in the expression of RUNX2 was also found, which represents the major transcription factor functional for the osteoblast differentiation,[51] regulating several bone-related genes.

As frequently reported in the literature,[52–55] the improvement in the cell behaviour observed for GL-coated scaffolds should be ascribed to the synergistic contribution of the surface chemistry, surface topography and roughness.

Finally, the peculiar characteristics of 3D AM scaffolds were preliminarily combined with the MAPLE deposition technique, thus allowing direct further research towards the development of smart and improved strategies for surface functionalization or combination of GL with other materials and 3D structures in a hybrid fashion for ensuring a tighter adhesion onto the substrates and improving cell behaviour, without altering the mechanical performance of the neat constructs.

However, in the field of regenerative medicine, the analysis of the inflammation process clearly represents a key aspect. In general, the inflammatory response potentially induced by a scaffold, including the release of inflammatory factors and the polarization of macrophages, could be studied in different ways. Just as an example, basal levels of inflammatory markers should be quantified adopting *in vitro* models of inflammation and measuring basal levels of different pro-inflammatory interleukins (*e.g.*, interleukin 1β (IL-1β)), interleukin-6 (IL-6) or anti – inflammatory interleukins (*e.g.*, interleukin-10 (IL-10)). A further methodology could be related to the investigation of specific signalling pathways (TLRs, NF-kB, MAPK, NLRP3, *etc.*) or M1-phenotype macrophage surface marker (Ccr7, CD86, and CD68) or M2-phenotype macrophage surface marker (CD163, Il-1rn, and Arg1) gene expression over the experimental period. Further improvements and strategies will be properly carried out in future studies.

Future efforts will be devoted to: (i) further studies for analysing and/or eventually optimizing the penetration depth of the MAPLE treatment, even if preliminary experimental tests already evidenced interesting results (data not shown), in terms of distribution of GL deposits inside the pores, *i.e.* on the scaffold fibre of the inner layers, due to the fully interconnected pore network; (ii) analysis of the disperse and polar components of the energy; (iii) investigation of the effect of different concentrations of GL suspension, analysis of the dose–response curves and the half maximal inhibitory concentration (IC50), as a measure of the potency of a substance in inhibiting a specific biochemical or biological process by half; (iv) the development of functionally graded structures for tissue repair and

regeneration, providing tailored properties at different scale levels, which could result from the combination of gradually distributed porosity, lattice architectures and material compositions.

Author contributions

Conceptualization: A. Gloria, T. Russo, M. Alfè and G. Ausanio. Data curation: T. Russo, A. Gloria and M. Alfè. Formal analysis: T. Russo, A. Gloria, V. Gargiulo and M. Alfè. Funding acquisition: G. Ausanio, A. Gloria and M. Alfè. Investigation: T. Russo, V. Peluso, and G. Ausanio. Methodology: T. Russo, V. Peluso, G. Ausanio, A. Gloria and M. Alfè. Supervision: G. Ausanio, A. Gloria and M. Alfè. Validation: T. Russo, V. Peluso, A. Gloria and M. Alfè. Writing – original draft and review & editing: T. Russo, V. Peluso, A. Gloria, V. Gargiulo and M. Alfè.

Conflicts of interest

There are no conflicts to declare.

Acknowledgements

The technical assistance of Mr Luciano Cortese for SEM analyses and Mr Rodolfo Morra for mechanical testing is gratefully acknowledged. The technical assistance of Dr Stefania Zeppetelli for biological analyses is also acknowledged. The research funding program of the University of Naples "Federico II" (Project title: CATe-GRAF, Fondo Ricerca di Ateneo—Linea B) is acknowledged for the financial support.

References

1 R. Pecci, S. Baiguera, P. Ioppolo, R. Bedini and C. Del Gaudio, *J. Mech. Behav. Biomed. Mater.*, 2020, **103**, 103583.
2 H. Qu, *Mater. Today Commun.*, 2020, **24**, 101024.
3 S. Cometa, M. A. Bonifacio, E. Tranquillo, A. Gloria, M. Domingos and E. De Giglio, *Polymers*, 2021, **13**, 150.
4 D. W. Hutmacher, *Biomaterials*, 2000, **21**, 2529–2543.
5 A. Gloria, B. Frydman, M. L. Lamas, A. C. Serra, M. Martorelli, J. F. Coelho, A. C. Fonseca and M. Domingos, *Mater. Sci. Eng., C*, 2019, **98**, 994–1004.
6 J. Groll, T. Boland, T. Blunk, J. A. Burdick, D.-W. Cho, P. D. Dalton, B. Derby, G. Forgacs, Q. Li and V. A. Mironov, *Biofabrication*, 2016, **8**, 013001.
7 R. Dhandapani, P. D. Krishnan, A. Zennifer, V. Kannan, A. Manigandan, M. R. Arul, D. Jaiswal, A. Subramanian, S. G. Kumbar and S. Sethuraman, *Bioact. Mater.*, 2020, **5**, 458–467.
8 T. Russo, V. Peluso, A. Gloria, O. Oliviero, L. Rinaldi, G. Improta, R. De Santis and V. D'Antò, *Nanomaterials*, 2020, **10**, 577.
9 A. Tampieri, T. D'Alessandro, M. Sandri, S. Sprio, E. Landi, L. Bertinetti, S. Panseri, G. Pepponi, J. Goettlicher and M. Bañobre-López, *Acta Biomater.*, 2012, **8**, 843–851.
10 N. Lewinski, V. Colvin and R. Drezek, *Small*, 2008, **4**, 26–49.
11 N. Singh, G. J. Jenkins, R. Asadi and S. H. Doak, *Nano Rev.*, 2010, **1**, 5358.
12 C. C. Berry and A. S. Curtis, *J. Phys. D: Appl. Phys.*, 2003, **36**, R198.
13 A. Gloria, T. Russo, U. d'Amora, S. Zeppetelli, T. d'Alessandro, M. Sandri, M. Bañobre-López, Y. Piñeiro-Redondo, M. Uhlarz and A. Tampieri, *J. R. Soc., Interface*, 2013, **10**, 20120833.
14 D. Ronca, F. Langella, M. Chierchia, U. D'Amora, T. Russo, M. Domingos, A. Gloria, P. Bartolo and L. Ambrosio, *Procedia CIRP*, 2016, **49**, 51–54.
15 R. De Santis, A. Gloria, T. Russo, U. d'Amora, S. Zeppetelli, C. Dionigi, A. Sytcheva, T. Herrmannsdörfer, V. Dediu and L. Ambrosio, *J. Appl. Polym. Sci.*, 2011, **122**, 3599–3605.
16 R. De Santis, A. Russo, A. Gloria, U. D'Amora, T. Russo, S. Panseri, M. Sandri, A. Tampieri, M. Marcacci and V. A. Dediu, *J. Biomed. Nanotechnol.*, 2015, **11**, 1236–1246.
17 U. D'Amora, T. Russo, A. Gloria, V. Rivieccio, V. D'Antò, G. Negri, L. Ambrosio and R. De Santis, *Bioact. Mater.*, 2017, **2**, 138–145.
18 C. Backes, A. Abdelkader, C. Alonso, A. Andrieux-Ledier, R. Arenal, J. Azpeitia, N. Balakrishnan, L. Banszerus, J. Barjon and R. Bartali, *2D Mater.*, 2020, **7**, 022001.
19 S. Saha, P. Lakhe, M. J. Mason, B. J. Coleman, K. Arole, X. Zhao, S. Yakovlev, S. Uppili, M. J. Green and R. A. Hule, *npj 2D Mater. Appl.*, 2021, **5**, 75.
20 U. Sierra, P. Álvarez, C. Blanco, M. Granda, R. Santamaría and R. Menéndez, *Carbon*, 2015, **93**, 812–818.
21 U. Sierra, P. Álvarez, C. Blanco, M. Granda, R. Santamaría and R. Menéndez, *Fuel*, 2016, **166**, 400–403.
22 U. Sierra, A. Mercado, E. Cuara, E. D. Barriga-Castro, A. Cortes, C. Gallardo-Vega and S. Fernandez, *Fuel*, 2020, **262**, 116455.
23 O. Vieira, R. S. Ribeiro, J. L. D. de Tuesta, H. T. Gomes and A. M. Silva, *Chem. Eng. J.*, 2022, **428**, 131399.
24 X. Kong, Y. Zhu, H. Lei, C. Wang, Y. Zhao, E. Huo, X. Lin, Q. Zhang, M. Qian and W. Mateo, *Chem. Eng. J.*, 2020, **399**, 125808.
25 N. Raghavan, S. Thangavel and G. Venugopal, *Appl. Mater. Today*, 2017, **7**, 246–254.
26 A. Poorna, R. Saravanathamizhan and N. Balasubramanian, *Electrochem. Sci. Adv.*, 2021, **1**, e2000028.
27 M. T.-u. Safian, U. S. Haron and M. M. Ibrahim, *BioResources*, 2020, **15**, 9756.
28 M. Olivi, M. Alfè, V. Gargiulo, F. Valle, F. Mura, M. Di Giosia, S. Rapino, C. Palleschi, D. Uccelletti and S. Fiorito, *J. Nanopart. Res.*, 2016, **18**, 1–10.
29 M. d'Amora, M. Alfe, V. Gargiulo and S. Giordani, *Nanomaterials*, 2020, **10**, 1472.
30 M. Alfe, G. Minopoli, M. Tartaglia, V. Gargiulo, U. Caruso, G. P. Pepe and G. Ausanio, *Nanomaterials*, 2022, **12**, 3663.
31 V. Gargiulo, M. Alfè, R. Di Capua, A. R. Togna, V. Cammisotto, S. Fiorito, A. Musto, A. Navarra, S. Parisi and A. Pezzella, *J. Mater. Chem. B*, 2015, **3**, 5070–5079.
32 F. Amantea, G. Antignani, G. Pota, E. Cascone, S. Parisi, M. Alfè, V. Gargiulo, G. Luciani, A. Pezzella and G. D'Errico, *Appl. Surf. Sci.*, 2023, 157608.

33 H.-S. Hung, A. Y.-H. Yu, S.-C. Hsieh, M.-L. Kung, H.-Y. Huang, R.-H. Fu, C.-A. Yeh and S.-H. Hsu, *ACS Appl. Mater. Interfaces*, 2020, **12**, 44393–44406.
34 S. Pandit, K. Gaska, R. Kádár and I. Mijakovic, *ChemPhysChem*, 2021, **22**, 250–263.
35 S. Noimark, C. W. Dunnill, M. Wilson and I. P. Parkin, *Chem. Soc. Rev.*, 2009, **38**, 3435–3448.
36 A. D. Stiff-Roberts and W. Ge, *Appl. Phys. Rev.*, 2017, **4**, 041303.
37 D. B. Chrisey, A. Piqué, R. A. McGill, J. S. Horwitz, B. R. Ringeisen, D. M. Bubb and P. K. Wu, *Chem. Rev.*, 2003, **103**, 553–576.
38 M. Alfè, V. Gargiulo, R. Di Capua, F. Chiarella, J. N. Rouzaud, A. Vergara and A. Ciajolo, *ACS Appl. Mater. Interfaces*, 2012, **4**, 4491–4498.
39 V. Gargiulo, B. Alfano, R. Di Capua, M. Alfé, M. Vorokhta, T. Polichetti, E. Massera, M. L. Miglietta, C. Schiattarella and G. Di Francia, *J. Appl. Phys.*, 2018, **123**, 024503.
40 M. A. Steiner and J. M. Fitz-Gerald, *Appl. Phys. A: Mater. Sci. Process.*, 2015, **119**, 629–638.
41 X. F. Wu and Y. A. Dzenis, *Acta Mech.*, 2006, **185**, 215–225.
42 H. Chen, H. Cheng, Z. Jiang, D. Qin, Y. Yu, G. Tian, F. Lu, B. Fei and G. Wang, *BioResources*, 2013, **8**, 2827–2838.
43 S. R. Moxon, M. J. S. Ferreira, P. Santos, B. Popa, A. Gloria, R. Katsarava, D. Tugushi, A. C. Serra, N. M. Hooper, S. J. Kimber, *et al.*, *Polymers*, 2020, **12**(7), 1478.
44 L. Ferroni, C. Gardin, F. Rigoni, E. Balliana, F. Zanotti, M. Scatto, P. Riello and B. Zavan, *Coatings*, 2022, **12**, 799.
45 M. Tabetah, A. Matei, C. Constantinescu, N. P. Mortensen, M. Dinescu, J. Schou and L. V. Zhigilei, *J. Phys. Chem. B*, 2014, **118**, 13290–13299.
46 M. Alfe, V. Gargiulo and R. Di Capua, *Appl. Surf. Sci.*, 2015, **353**, 628–635.
47 A. Kozbial, Z. Li, C. Conaway, R. McGinley, S. Dhingra, V. Vahdat, F. Zhou, B. D'Urso, H. Liu and L. Li, *Langmuir*, 2014, **30**(28), 8598–8606.
48 C. Shuxiang, W. Chuanxiang, Y. Wenguang, L. Wenfeng, Y. Haibo and L. Lianqing, *Nanotechnol. Rev.*, 2020, **9**(1), 971–989.
49 V. M. Villapun Puzas, L. N. C. Arter, C. Schröder, P. E. Colavita, D. A. Hoey, M. A. Webber, O. Addison, D. E. T. Shepherd, M. M. Attallah, L. M. Grover and S. C. Cox, *ACS Biomater. Sci. Eng.*, 2022, **8**(10), 4311–4326.
50 S. Bailey, G. Karsenty, C. Gundberg and D. Vashishth, *Ann. N. Y. Acad. Sci.*, 2017, **1409**, 79–84.
51 S. Chen, J. Gluhak-Heinrich, Y. Wang, Y. Wu, H. H. Chuang, L. Chen, G. Yuan, J. Dong, I. Gay and M. MacDougall, *J. Dent. Res.*, 2009, **88**, 904–909.
52 F. Lin, F. Du, J. Huang, A. Chau, Y. Zhou, H. Duan, J. Wang and C. Xiong, *Colloids Surf., B*, 2016, **146**, 785–793.
53 Q. Wang, Y. Chu, J. He, W. Shao, Y. Zhou, K. Qi, L. Wang and S. Cui, *Mater. Sci. Eng., C*, 2017, **80**, 232–242.
54 P. Ginestra, *J. Mech. Behav. Biomed. Mater.*, 2019, **100**, 103387.
55 J. Guo, G. Cao, S. Wei, Y. Han and P. Xu, *Heliyon*, 2023, **9**(11), e21872.